UNITED NATIONS EDUCATIONAL, SCIENTIFIC AND CULTURAL ORGANIZATION
INTERNATIONAL ATOMIC ENERGY AGENCY
INTERNATIONAL CENTRE FOR THEORETICAL PHYSICS
I.C.T.P., P.O. BOX 586, 34100 TRIESTE, ITALY, CABLE: CENTRATOM TRIESTE

H4.SMR/1058-12

WINTER COLLEGE ON OPTICS

9 - 27 February 1998

Ultrafast Pulsed Signals - Methods of Diagnostics, Recording, Retrieval and Design

P. Saari

Institute of Physics, University of Tartu, Estonia

MAIN BUILDING STRADA COSTIERA, 11 TEL. 2240111 TELEFAX 224163 TELEX 460392 ADRIATICO GUEST HOUSE VIA GRIGNANO, 9 TEL. 224241 TELEFAX 224531 TELEX 460449
MICROPROCESSOR LAB. VIA BEIRUT, 31 TEL. 2249911 TELEFAX 224600 TELEX 460392 GALILEO GUEST HOUSE VIA BEIRUT, 7 TEL. 2240311 TELEFAX 2240310 TELEX 460392
ENRICO FERMI BUILDING VIA BEIRUT, 6 (TELEPHONE, FAX AND TELEX THROUGH MAIN BUILDING)

Winter College on Optics 1998

"Ultrafast pulsed signals - methods of diagnostics, recording, retrieval and design "

Prof. Peeter Saari

Institute of Physics, University of Tartu,

Estonia

http://www.fi.tartu.ee/Saari

Outline - Controversial meaning of 'time-dependent spectrum'. Time-frequency representations of signals: from music score to Wigner distribution. Time response of a spectrometer. Optical spectro(chrono)gram. Impossibility of optical oscilloscope and phase retrieval problem. FROG: frequency resolved optical gating. 'Holographist's rule' to overcome optical phase loss. Time-domain holography. Pulse shaping by spectral holography and spectral hole burning. Spread-free Bessel-X femtosecond pulses.

Fourier transforms

$f(t)=\frac{1}{2\pi}\int_{-\infty}^{\infty}F(\omega)e^{i\omega t}d\omega$	Re $f(t)$	Re $F(\omega)$, $\lvert F(\omega)\rvert$	$\lvert F(\omega)\rvert^2$	arg $F(\omega)$	$F(\omega)=\int_{-\infty}^{\infty}f(t)e^{-i\omega t}dt$
$\exp\left[-\frac{1}{2}t^2\right]-\exp\left[-\frac{1}{2}\left(\frac{t}{1/8}\right)^2\right]$	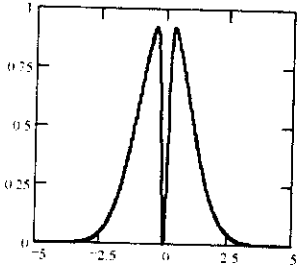	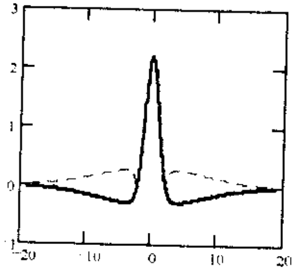	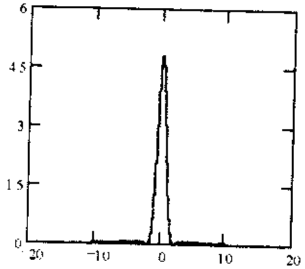	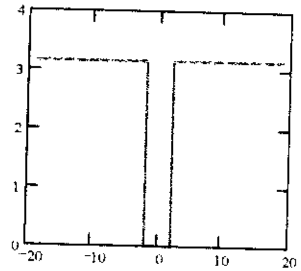	$\sqrt{2\pi}\exp\left[-\frac{1}{2}\omega^2\right]-\frac{\sqrt{2\pi}}{8}\exp\left[-\frac{1}{2}\left(\frac{\omega}{8}\right)^2\right]$
$\exp\left[-\frac{1}{2}\left(\frac{t-1}{1/8}\right)^2\right]$	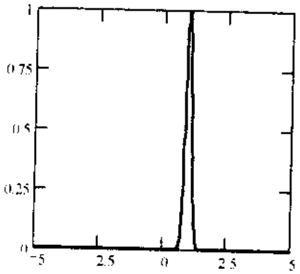	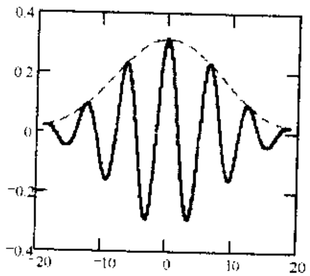	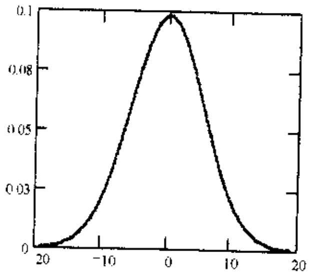	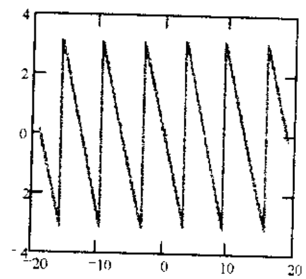	$\frac{\sqrt{2\pi}}{8}\exp\left[-\frac{1}{2}\left(\frac{\omega}{8}\right)^2-i\omega\right]$
$\Pi_3(t)\cos 12t$	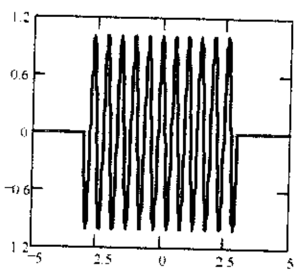	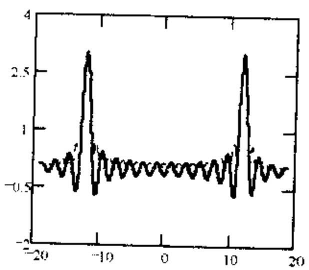	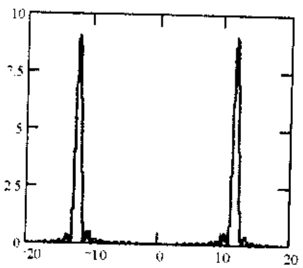	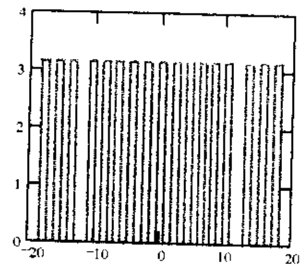	$\frac{\sin 3(\omega+12)}{(\omega+12)}+\frac{\sin 3(\omega-12)}{(\omega-12)}$
$Y(t)\exp(-\frac{t}{3}+i\cdot 8t)$	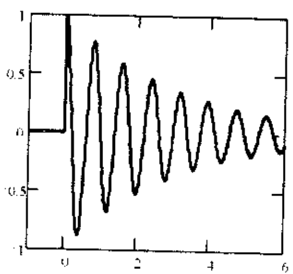	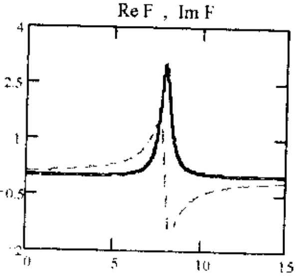	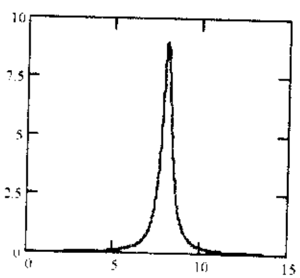	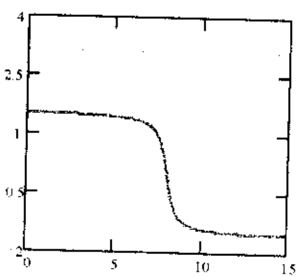	$\frac{1}{i(\omega-8)+\frac{1}{3}}$

RESPONSES OF LINEAR TIME-INVARIANT SYSTEMS

Pulse response:

$$y(t) \;=\; \mathcal{N}\{x(t)\} \;\equiv\; \int d\tau\, h(\tau)\, x(t-\tau) \;\equiv\; h(t) \otimes x(t) \quad .$$

Frequency response:

$$Y(\omega) \;=\; H(\omega)\cdot X(\omega) \quad .$$

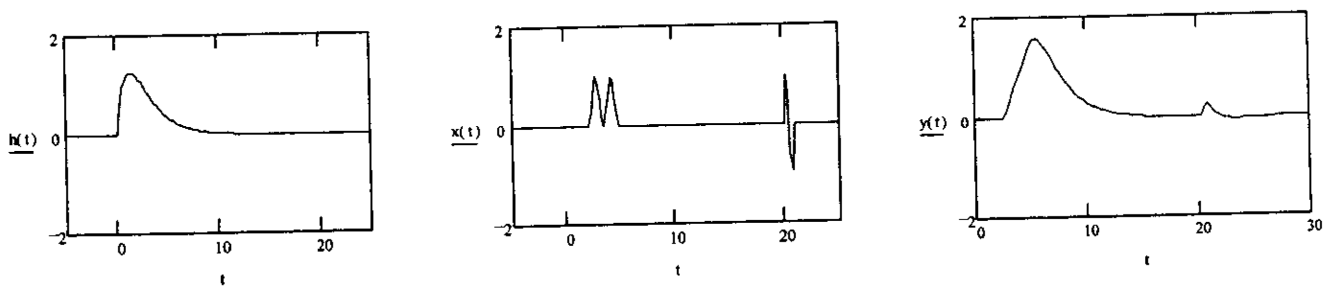

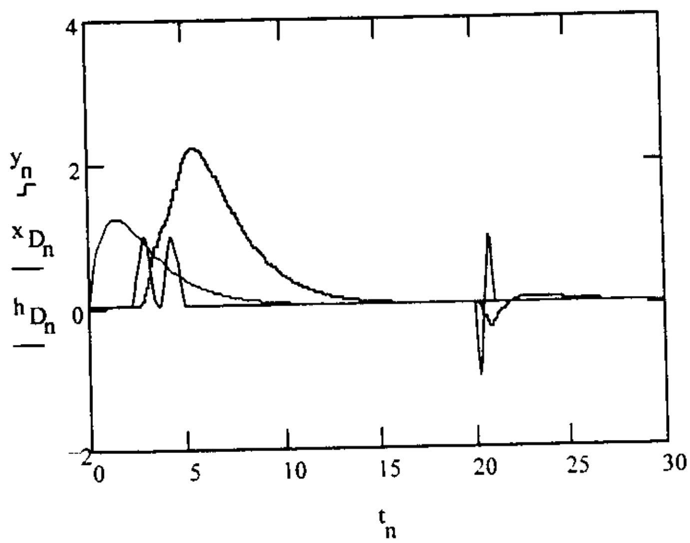

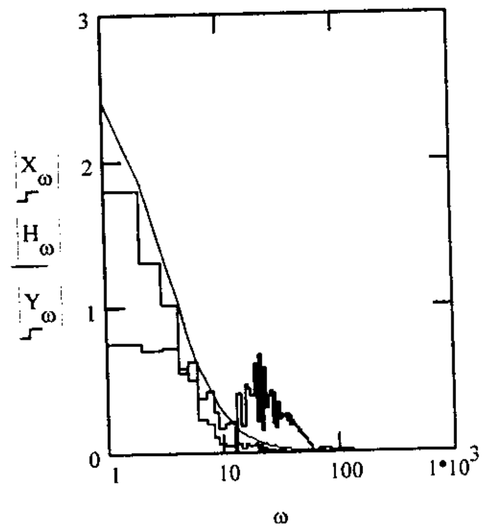

2-D TIME-FREQUENCY REPRESENTATIONS OF 1-D SIGNALS

Gabor transform:

$$\hat{G}\left\{s(t)\right\} \equiv \int_{-\infty}^{\infty} s(t)g(t-\tau)e^{-i\omega t}dt$$

Spectrogram *(with example)*:

$$S(\omega,\tau) = \hat{F}_{gated}\left\{s(t)\right\} \equiv \left|\int_{-\infty}^{\infty} s(t)g(t-\tau)e^{-i\omega t}dt\right|^2$$

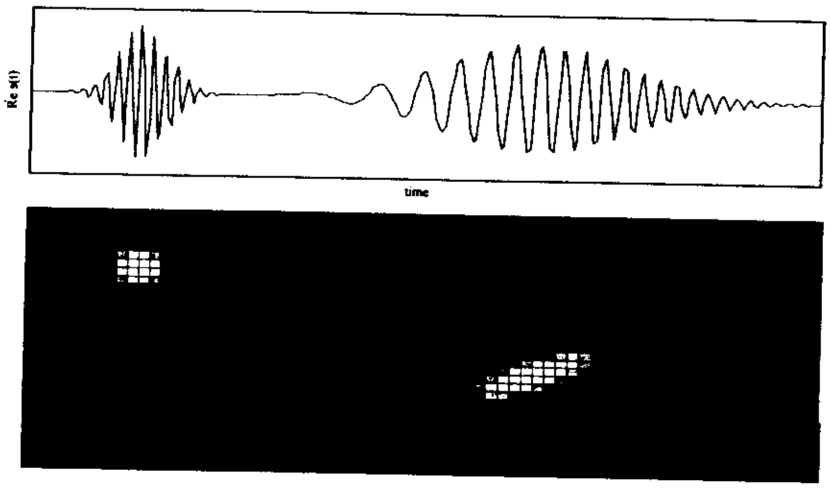

Wigner-Ville distribution:

$$W(\omega,\tau) = \tfrac{1}{2\pi}\int_{-\infty}^{\infty} dt\, s^*(\tau - \tfrac{1}{2}t)\, s(\tau + \tfrac{1}{2}t)e^{-i\omega t}$$

$$\int W(\omega,\tau)d\omega = \left|s(\tau)\right|^2 \quad \int W(\omega,\tau)d\tau = \left|S(\omega)\right|^2$$

Discrete Gabor transform

$$G_{mn} = \hat{G}_D\left\{s(t)\right\} \equiv \int_{-\infty}^{\infty} s(t)g(t-nD_t)e^{-imD_\omega t}dt$$

Picosecond Spectrochronography

ARVI FREIBERG AND PEETER SAARI

Abstract—The general problem of extracting complete (amplitude and phase) information out of an optical signal is discussed. We have shown that the best one can do to determine all essential features of light pulses is to apply simultaneous temporal and spectral analysis to take spectrochronograms with the appropriate shape of the resolution cell on the ωt-plane. We use the term "spectrochronogram" instead of the much broader term "time-resolved spectrum" for a specific measurement result where the resolutions $\Delta\omega$ and Δt used are transform correlated. A novel subtractive mount of monochromators has been proposed to overcome the obstacles to experimental realization of uncertainty-principle-limited setups for high spectral resolution picosecond spectrochronography. For the examples of perylene and anthracene molecules, experimental spectrochronograms revealing temporal behavior of hot luminescence lines and, correspondingly, picosecond kinetics of intramolecular vibrational relaxation have been presented. Some further applications of picosecond spectrochronography have been discussed.

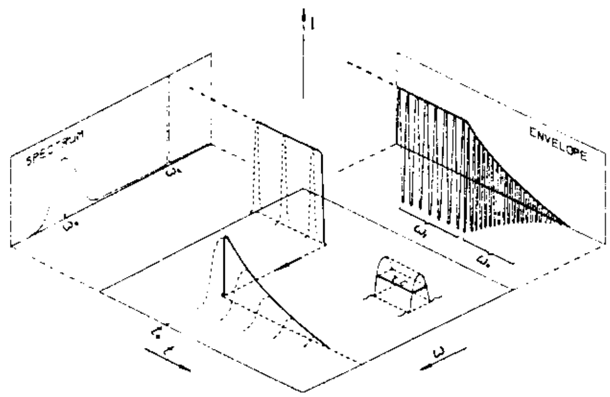

Fig. 1. Right-hand side: the wave emitted by a damped oscillator in case of a sinusoidal driving force. At $t = t_0$, the driving force is abruptly turned off and the forced vibration turns into free decaying vibration at the natural (resonance) frequency ω_0. Left-hand side: the spectrum of the wave. Foreground: the solid curve—the trajectory in the $\omega t I$-space representing the temporal behavior of the amplitude and carrier frequency of the wave; dashed curves—intersections of an imaginable "instantaneous spectrum." The rectangle rc depicts a Gabor-type resolution cell of an area $\Delta\omega \cdot \Delta t = 2\pi$, which may be ascribed to a prism or grating spectrograph with the response duration Δt (and, correspondingly, sinc-function-shaped spectral response of FWHM = $\Delta\omega$).

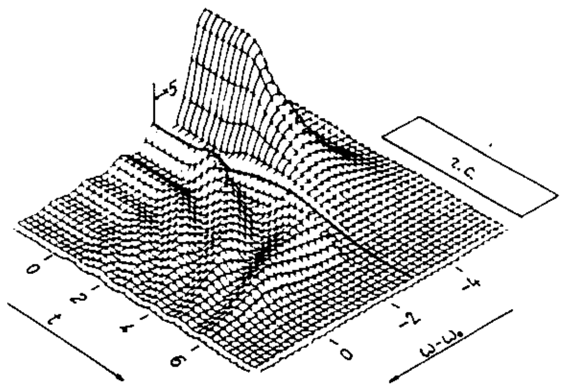

Fig. 2. Spectrochronogram, calculated for the model situation of Fig. 1. Right-hand side: the resolution cell corresponding to $\Delta t = 6$ is shown. The oscillator decay constant has been taken as a time unit, its reciprocal, as a unit for the emission frequency $\omega - \omega_0$. After the driving force of a frequency $\omega_1 = \omega_0 - 4$ is switched off at $t = 0$, one can observe a nonmonotonic behavior of the intensity around the emitter frequency, which transforms into an exponentially decaying Lorentzian-like band at $t = 6$, i.e., after the spectrograph has forgotten the carrier frequency jump.

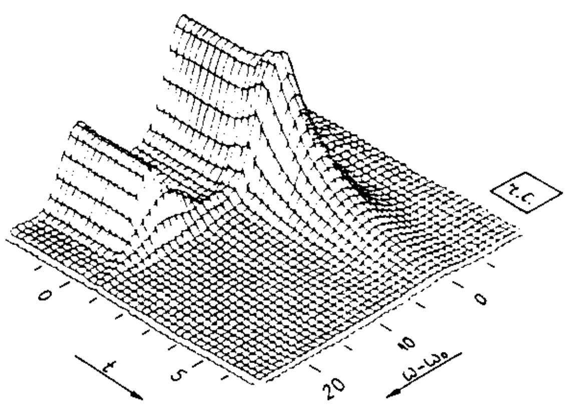

Fig. 3. Spectrochronogram calculated according to (1a) for the secondary light emission of an ensemble of two-level systems subjected to excitation by a long, but weak, rectangular laser pulse and, unlike the previous example, impact-type relaxation. As compared to Fig. 2, the excitation frequency detuning is much larger ($\omega_1 - \omega_0 = 16$) and of the opposite sign (to place the trajectory of forced vibrations, i.e., of scattered light in the forefront). After the driving field is switched off at $t = 0$, the scattering dies out within $\Delta t = 1$ (chosen equal to

ELIMINATION OF EXCESS PULSE BROADENING AT HIGH SPECTRAL RESOLUTION OF PICOSECOND DURATION LIGHT EMISSION

P. SAARI, J. AAVIKSOO, A. FREIBERG and K. TIMPMANN

ELIMINATION OF EXCESS PULSE BROADENING AT HIGH SPECTRAL RESOLUTION OF PICOSECOND LIGHT PULSES

P.Saari, J.Aaviksoo, A.Freiberg, and K.Timpmann

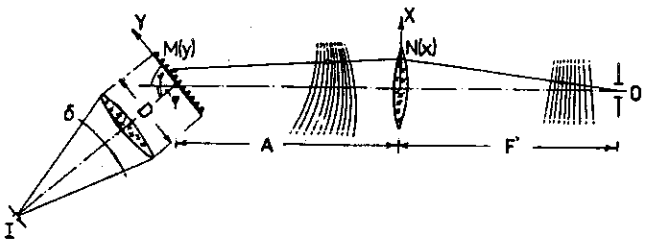

Fig.2. To the direct evaluation of monochromator response function. Wavepacket formation from the δ-pulse on the grating and its spreading toward the exit slit are shown. The leading front of the packet is born on the right edge of the grating and the rear front on the left edge resulting in the frequency decrease with the angle increase

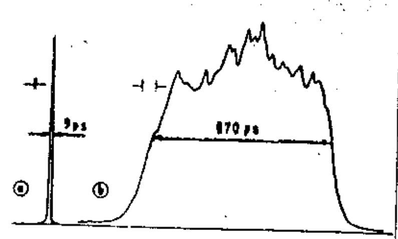

Fig. 4. a) Temporal response of a subtractive dispersion double monochromator (600 grooves/mm; $M = 1:2,5$; spectral width of the intermediate slit 7 cm^{-1}) showing the narrowing effect. b) Response of a common Raman-quality double monochromator DFS-24 (1200 grooves/mm, $M = 1:5$). FWHMs of streak-camera responses are indicated.

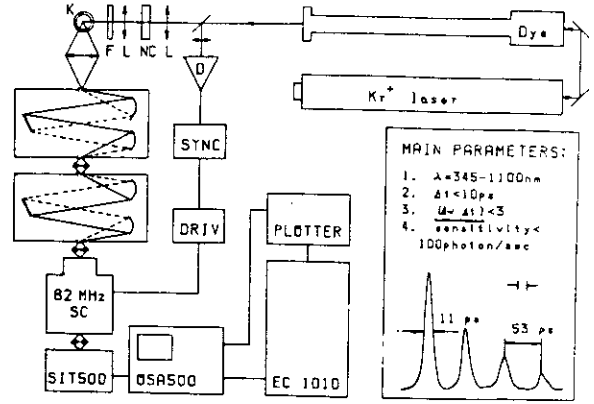

spectrochronography: $\Delta\omega \cdot \Delta t \gtrsim 1$

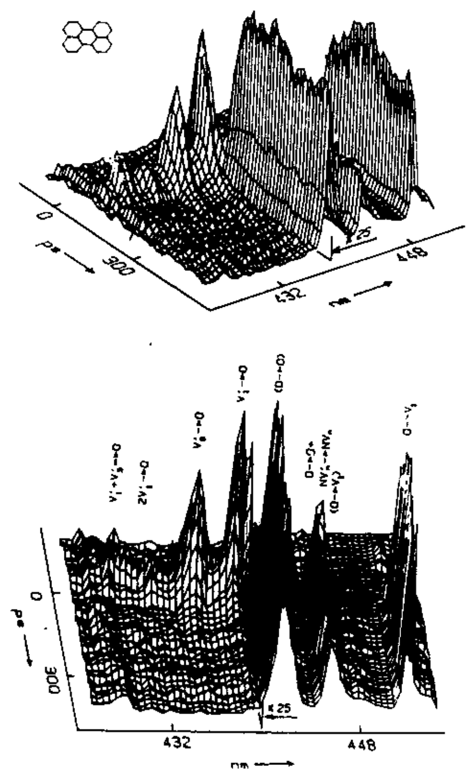

FIGURE 2. Two views of the spectrochronogram of the fluorescence of perylene molecules (near 0–0 transition region) in the n-heptane matrix at 4.2 K. The spectral width of the intermediate slit is 31 cm^{-1}. At $t = 0$ an excitation by tightly-focused nearly transform-limited (3 ps long and 5 cm^{-1} spectrally wide) frequency-doubled laser pulses (average power density 6–30 W/cm^2) at λ = 393.8 nm populate a selected high-lying intramolecular vibrational level of S_1 manifold.

The FROG trace is a spectrogram of E(t).

Substituting for $E_{sig}(t,\tau)$:

$$E_{sig}(t,\tau) \propto E(t)\,|E(t-\tau)|^2$$

$$I_{FROG}(\omega,\tau) \propto \left| \int_{-\infty}^{+\infty} E_{sig}(t,\tau)\, \exp(-i\omega t)\, dt \right|^2$$

yields:

$$I_{FROG}(\omega,\tau) \propto \left| \int_{-\infty}^{+\infty} E(t) \qquad \exp(-i\omega t)\, dt \right|^2$$

Unfortunately, spectrogram inversion algorithms require that we know the gate function.

Instead, consider FROG as a two-dimensional phase-retrieval problem.

If $E_{sig}(t,\Omega)$ is the 1-D Fourier transform of the signal field, $E_{sig}(t,\tau)$, with respect to delay, τ, then:

The input pulse field, E(t), is easily obtained from $E_{sig}(t,\Omega)$.

and

$$I_{FROG}(\omega,\tau) \propto \left| \int_{-\infty}^{+\infty} \int_{-\infty}^{+\infty} E_{sig}(t,\Omega)\, \exp(-i\omega t - i\Omega\tau)\, dt\, d\Omega \right|^2$$

Measuring ultrashort laser pulses in the time-frequency domain using frequency-resolved optical gating

Rick Trebino, Kenneth W. DeLong, David N. Fittinghoff, John N. Sweetser, Marco A. Krumbügel, and Bruce A. Richman
Combustion Research Facility, Sandia National Labs, Livermore, California 94550

Daniel J. Kane
Southwest Sciences, Incorporated, Suite E-11, 1570 Pacheco Street, Santa Fe, New Mexico 87501

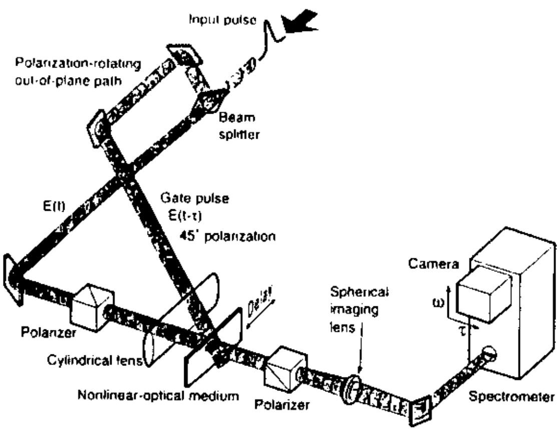

FIG. 6. Experimental apparatus for single-shot PG FROG [from Kane and Trebino (Ref. 21)]. In order to perform a single-shot measurement, the beams are crossed at a large angle (10–20 deg) and focused with a cylindrical lens, yielding a line focus in the nonlinear medium, where the relative delay between the two pulses varies with spatial coordinate along the line focus. This focus is then imaged onto the entrance slit of the spectrometer, whose output yields the entire FROG trace on a single shot. In this apparatus, the out-of-plane propagation of one of the beams is to rotate the polarization of the beam by about 45 deg.

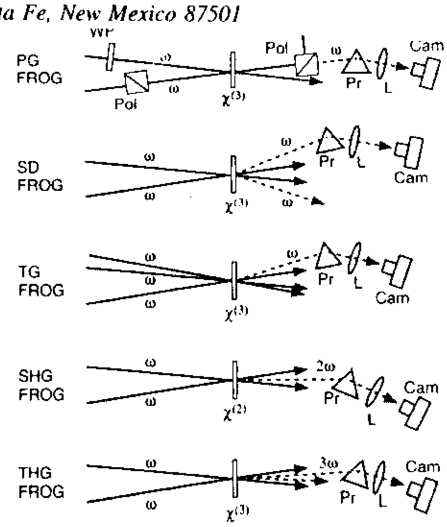

FIG. 1. Schematics of five different beam geometries for performing FROG measurements of ultrashort laser pulses: polarization gate (PG), self-diffraction (SD), second-harmonic generation (SHG), and third-harmonic generation (THG), and transient grating (TG) FROG. Solid lines indicate input pulses, and dashed lines indicate signal pulses. The nonlinearity of the nonlinear medium is shown; Pol=polarizer; WP=wave plate; Pr=prism; L=lens; and Cam=Camera. The prism-lens combination in each arrangement is meant to represent a generic spectrometer, which could involve a grating or other dispersive element instead of the prism. Not shown are delay lines and various additional lenses, also common to all arrangements. The frequencies shown (ω, 2ω, 3ω) are the carrier frequencies of the pulses involved and indicate whether the signal pulse has the same carrier frequency as the input pulse or is shifted, as in SHG and THG.

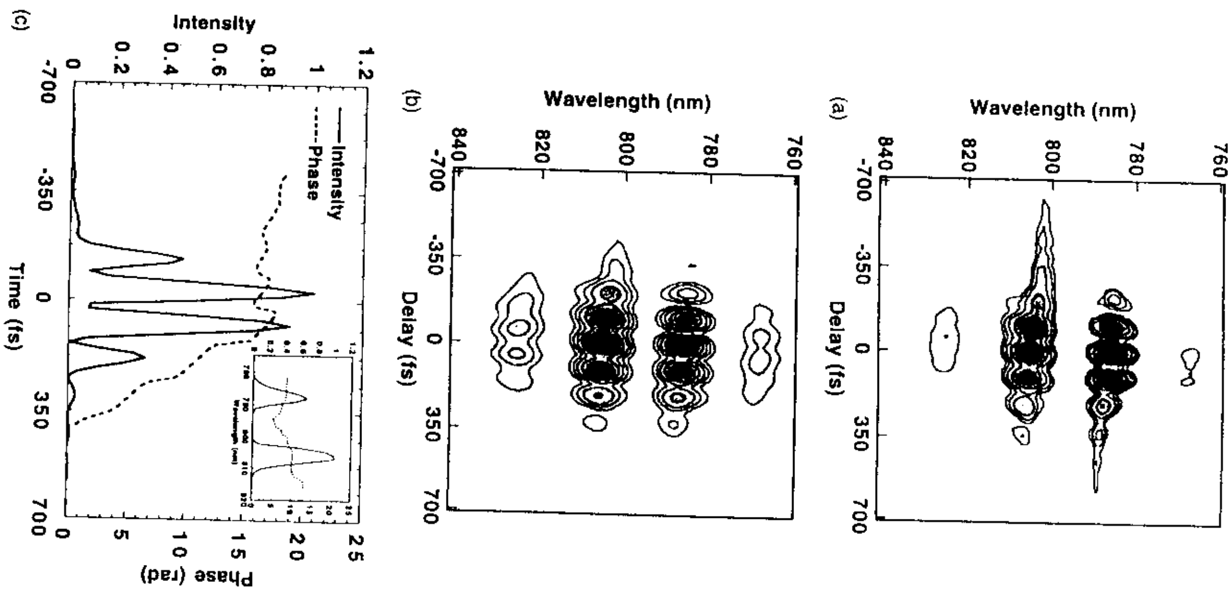

FIG. 5. (a) Experimental multishot FROG trace for a shaped (multiple pulse) ultrashort laser pulse. (b) FROG trace for the pulse retrieved by the algorithm. (c) Retrieved intensity and phase. Note that FROG is able to retrieve a pulse that is quite complex. (Discrepancies between the measured and retrieved traces are probably due to spatial inhomogeneities in the beam.)

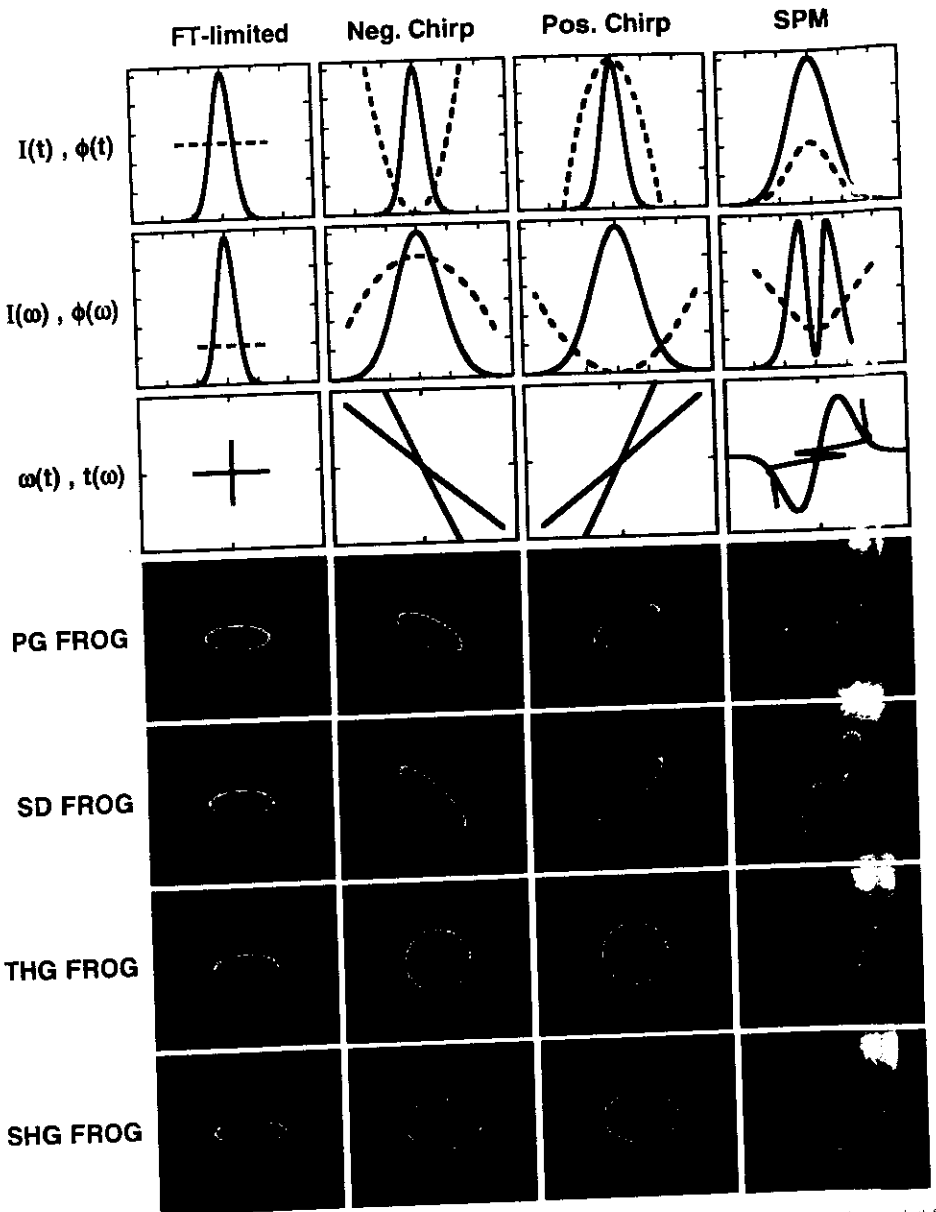

FIG. 2. FROG traces for the various FROG geometries for typical ultrashort light pulses. The top row shows the intensity vs time, $I(t)$ (solid line), and phase vs time, $\varphi(t)$ (dashed line), for various pulses. The next row shows the spectrum, $\tilde{I}(\omega-\omega_0)$ (solid line), and the spectral phase, $\tilde{\varphi}(\omega-\omega_0)$ (dashed line), for each pulse. In the first two rows of plots in this figure, the ticks on the phase axis correspond to increments of π radians. The third row shows the instantaneous frequency vs time, $\omega(t)$ (in blue). Also shown in the third row is the group delay vs frequency, $\tilde{\tau}(\omega)$ (in green). Note that the $\tilde{\tau}(\omega)$ plots must be turned sideways because the horizontal axis in this row of figures is time, and the vertical axis is frequency. Arrows in this figure indicate infinities. The remaining four rows show false-color (purple means high intensity and red means low intensity) FROG traces for the various pulses for the different FROG beam geometries: polarization gate (PG), self-diffraction (SD), second-harmonic generation (SHG), and third-harmonic generation (THG). Note that no row exists for transient grating (TG) FROG because it yields traces that are identical to PG FROG or SD FROG, depending on which pulse is delayed. Note that the PG and SD FROG traces mirror the instantaneous frequency vs time or the group delay vs frequency, whichever is more intuitive. The THG FROG traces are more symmetrical, and hence less intuitive, and the SHG FROG traces are perfectly symmetrical and hence have an ambiguity in the direction of time.

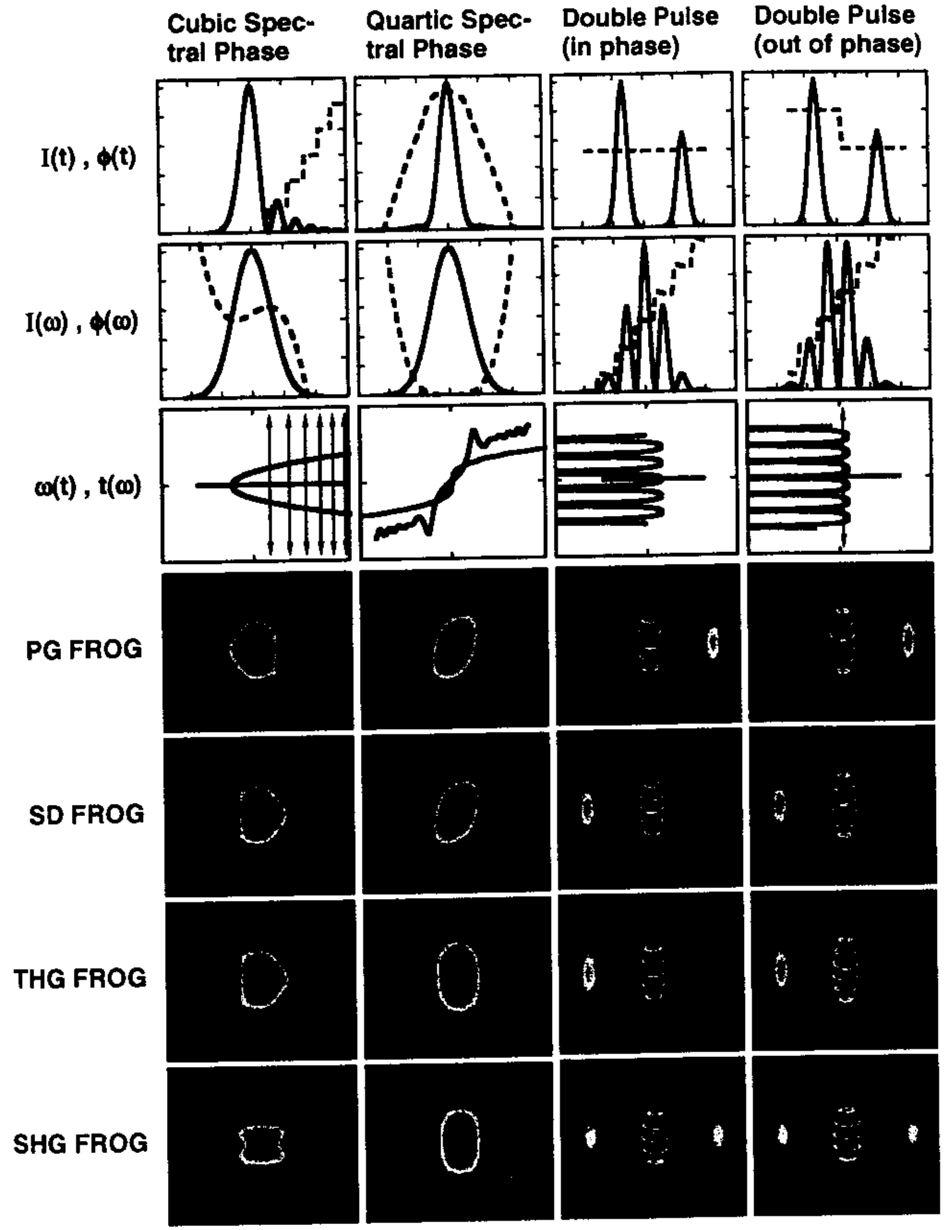

FIG. 2 (*Continued.*)

Generalized Projections

A projection maps the current guess for the waveform to the closest point in the constraint set.

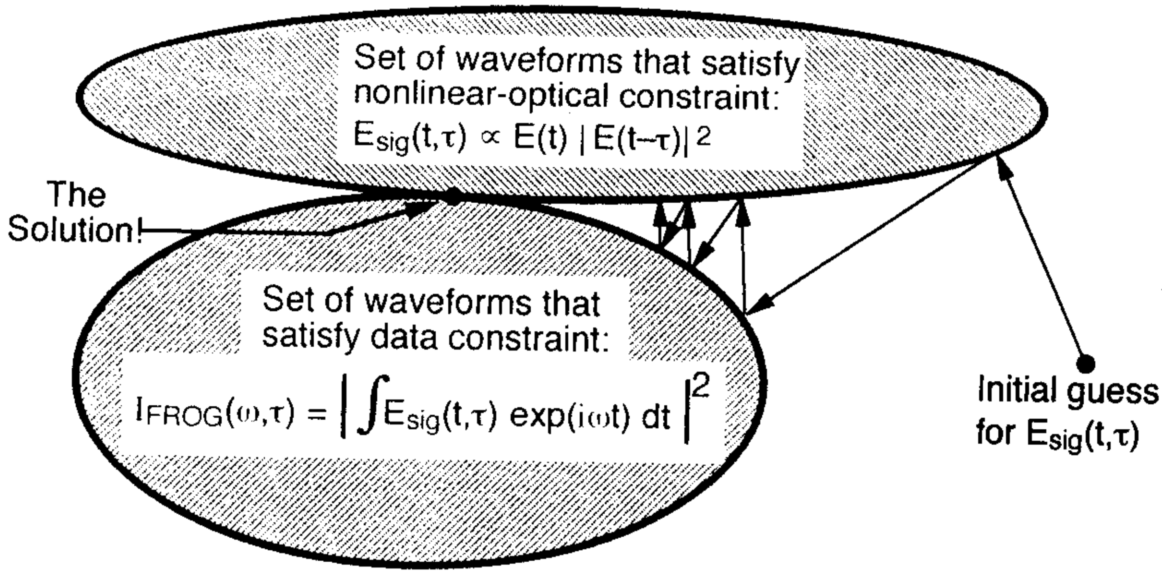

Convergence is guaranteed for convex sets, but generally occurs even with nonconvex sets.

New, Improved Generic Ultrafast Measurement

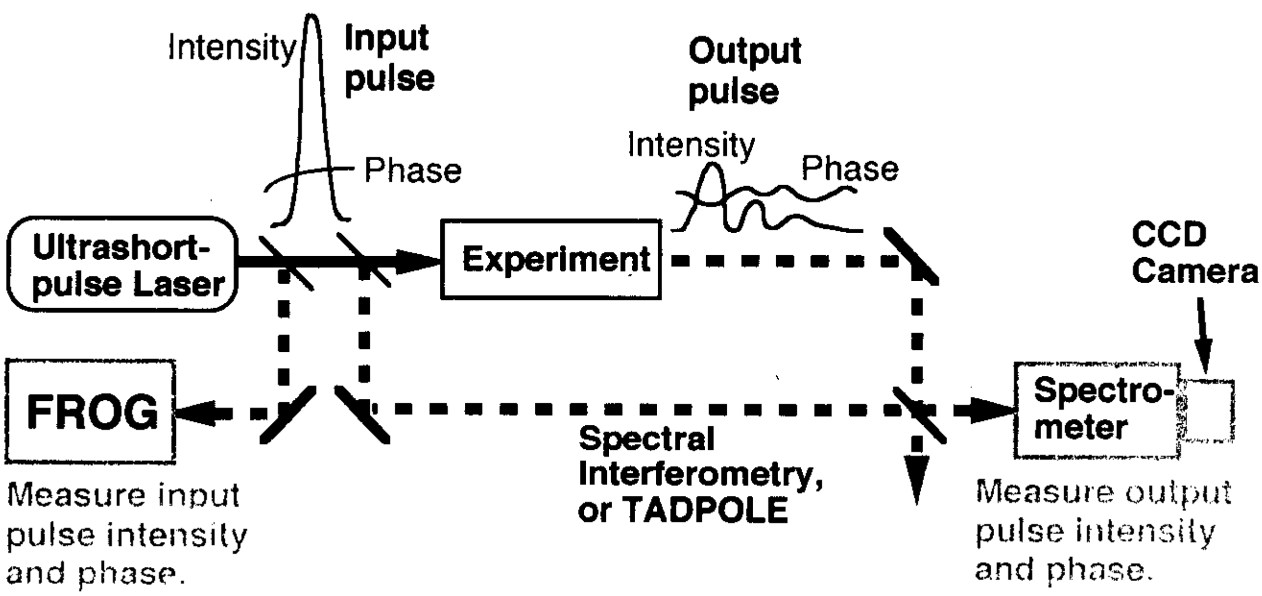

Sensitivity is approximately that of simple energy-detector, but with much more information.

TIME–DOMAIN HOLOGRAPHY

Rebane, Kaarli and Saari, JETP Lett.20,320 (1983)

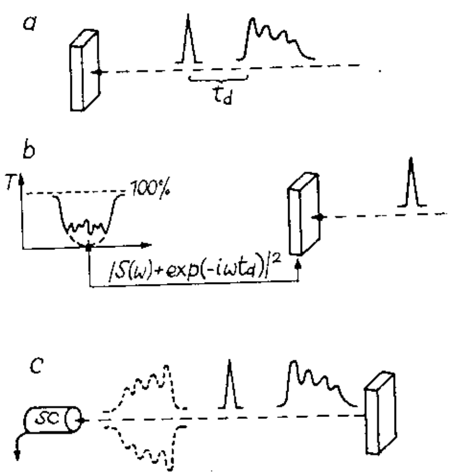

STREAK–CAMERA TRACES :

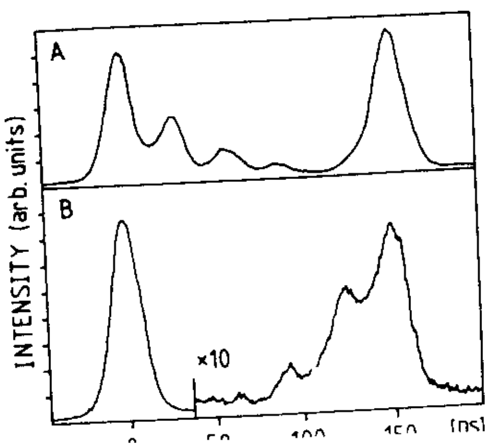

PHOTOCHEMICAL HOLE BURNING

I CW PHB → single narrow (~10^{-4} Å) holes — A. Gorokhovski, R. Kaarli, L. Rebane, JETP Lett. 20, 216, 1974; B. Kharlamov, R. Personov, L. Bykovskaja, Opt. Comm. 12, 191, 1974

II pulsed PHB → spectral hologram, — A. Rebane, R. Kaarli, P. Saari, Opt. Spectr. 55, 405, 1983

READ IN $S(t)$

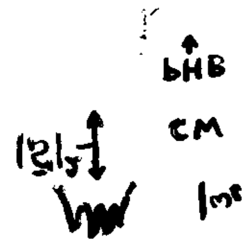

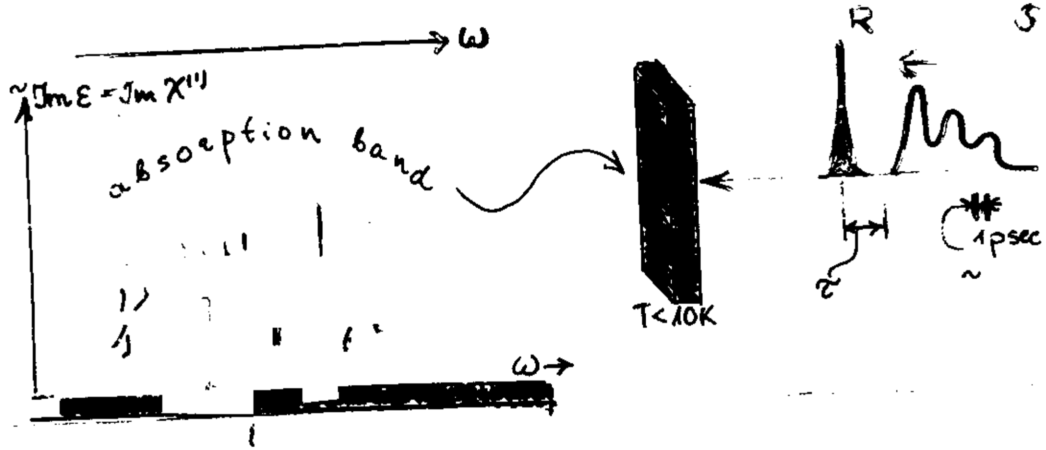

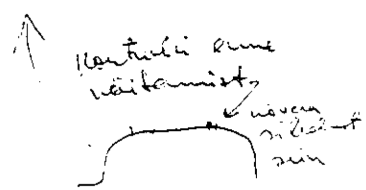

Spectral [illegible] burnt into ε of sample

$$\mathrm{Im}\,\varepsilon \sim |\bar{R}+\bar{S}|^2 \sim R^2+|S(\omega)|^2+Re^{i\omega\tau}S(\omega)+Re^{-i\omega\tau}S^*(\omega)$$

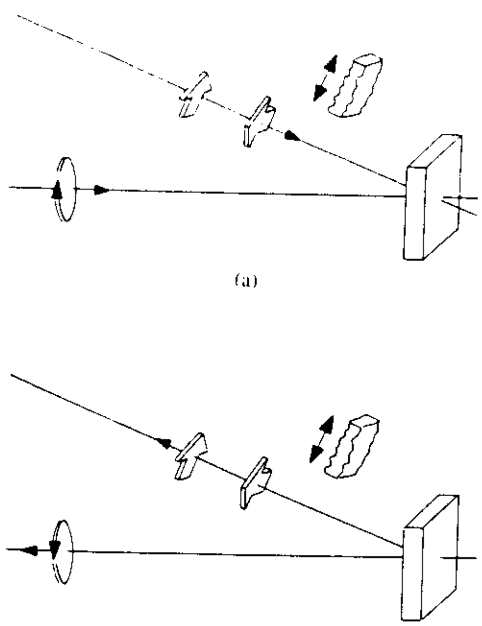

(a)

(b)

Fig. 4. Schematic of recording (a) and conjugated reconstruction (phase conjugation) (b). The oblique object beam consists of two temporally-separated and spatially-partly-overlapping picosecond pulses of orthogonal linear polarizations. The cross section of the wavefronts of the pulses is shaped by arrow-like transmission masks, while the direction of the arrows corresponds to the polarization plane. Plane reference and reading pulses are of counterrotating circular polarizations.

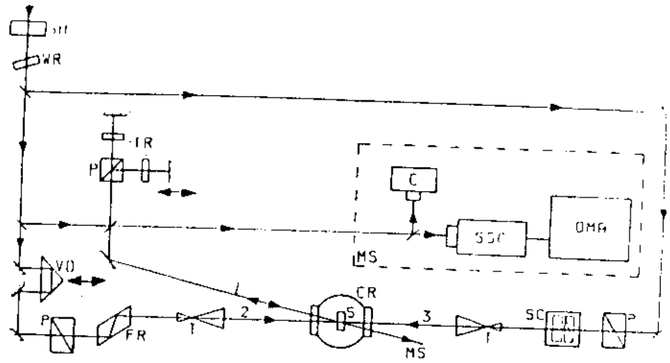

Fig. 2. Experimental setup. SH: shutter, WR: wave retarder, VD: variable delay, P: prism polarizer, FR: Fresnel rhomb, T: telescope, SC: Babinet-Soleil compensator, TR: arrow-shaped transparencies, CR: cryostat, S: sample, MS: measuring system, C: camera, SSC: synchroscan streak camera, OMA: optical multichannel analyzer. 1: object beam, 2: plane reference beam which was used for reading the hologram in the course of direct reconstruction, 3: readout beam for conjugated reconstruction.

(a) (b) (c)

Fig. 5. Analysis of the images in the experiments on phase conjugation without distorter. (a) Image of the reconstructed wave at the output of interferometer. (b) and (c) The same with perpendicular orientations of the analyzer. The correction for distortions introduced by diffraction on transmission masks can be seen.

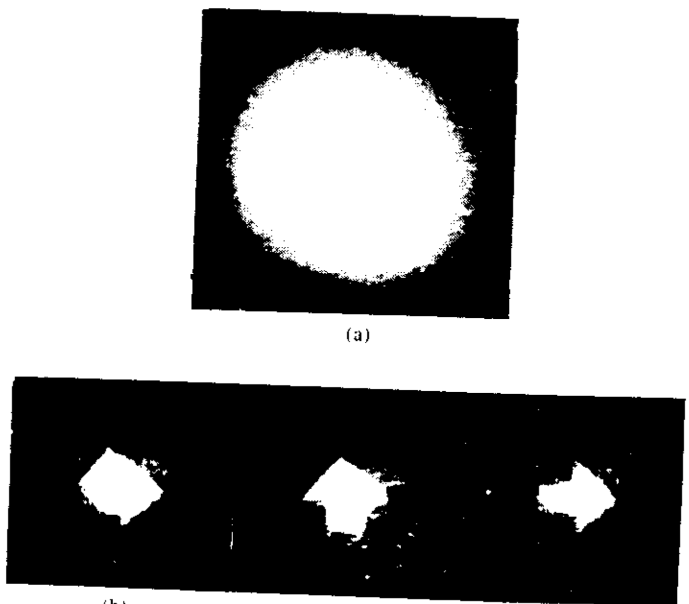

(a)

(b) (c) (d)

Fig. 6. Analysis of the images in the experiments on phase conjugation with distorter. (a) Distorted wave. (b) Reconstructed wave after reverse propagation through the distorting medium with the analyzer removed. (c) and (d) The same with perpendicular orientations of the analyzer.

IEEE JOURNAL OF QUANTUM ELECTRONICS, VOL. 28, NO. 10, OCTOBER 1992 2231

Femtosecond Spectral Holography

Andrew M. Weiner, *Senior Member, IEEE*, Daniel E. Leaird, David H. Reitze, and Eung Gi Paek

Invited Paper

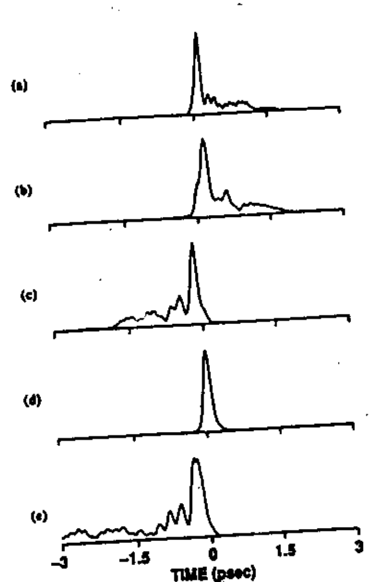

Fig. 5. Intensity cross-correlation measurements, showing holographic storage and recall of a signal pulse distorted via cubic spectral phase modulation. The curves are individually normalized for the same height. (a) Input signal pulse. (b) Real reconstructed output pulse ($\bar{k}_r = \bar{k}_s$). (c) Time-reversed output pulse ($\bar{k}_r = \bar{k}_s$). (d) Autocorrelation of the signal field, obtained using a test pulse identical to the signal pulse (with $\bar{k}_t = \bar{k}_s$). The peak is actually 1.6× stronger than that in (c). (e) Time-reversed autoconvolution of the signal field, obtained using a test pulse time-reversed with respect to the signal pulse (with $\bar{k}_t = \bar{k}_s$). The peak is actually 2× weaker than that in (c).

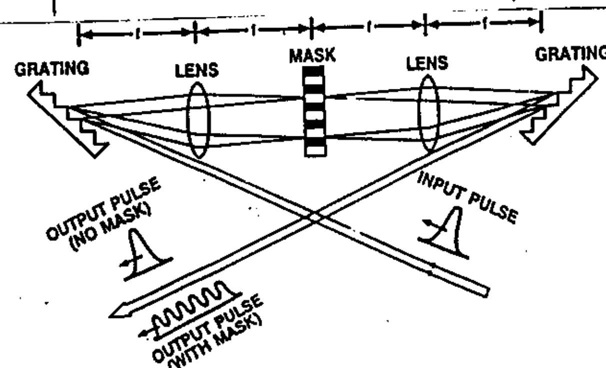

Fig. 1 Femtosecond pulse shaping apparatus (from ref. 9).

13

17

PULSE SHAPING (time-domain ...

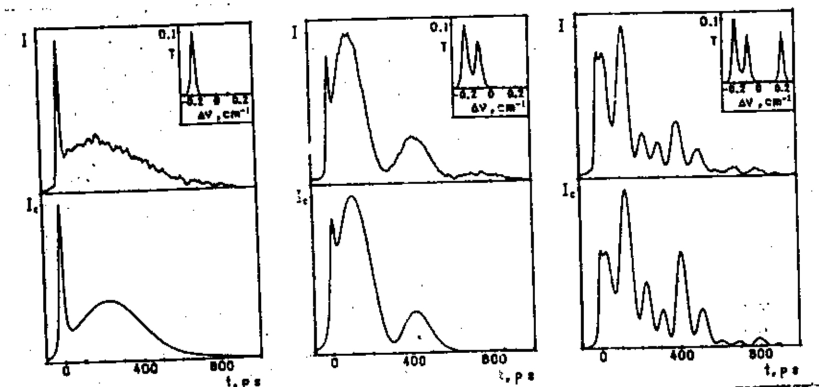

$$R(t) = \hat{F}\Big[\,T(\omega)\cdot\exp\Big[\,i\hat{H}\big[\ln T(\omega)\big]\Big]\Big], \quad \text{where}$$

R – output pulse, $\hat{F}$ & $\hat{H}$ – Fourier & Hilbert transform...

$T(\omega)$ – (spectral) amplitude transmittance of the elem...

OPTICAL PULSE SHAPING BY FILTERS BASED ON SPECTRAL HOLE BURNING

H. SÕNAJALG, A. GOROKHOVSKII, R. KAARLI, V. PALM, M. RÄTSEP and P. SAARI

Volume 71, number 6 OPTICS COMMUNICATIONS 15 June 1...

Simple monochromatic 'diffraction-free' field
– sum of two plane waves:

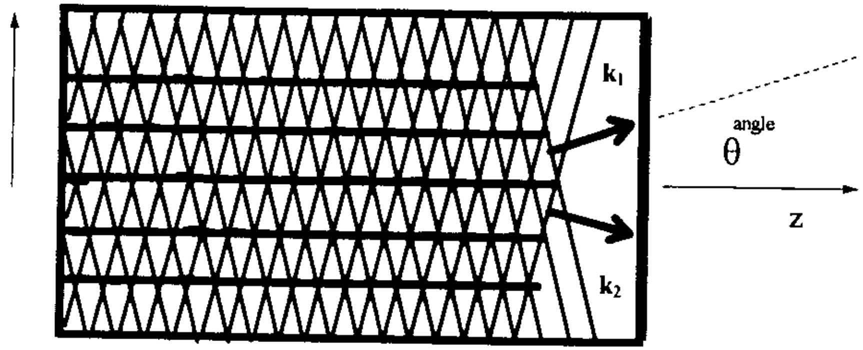

$$e^{i(k_x x + k_z z)} + e^{i(-k_x x + k_z z)} \quad \propto \quad \cos k_x x \cdot e^{ik_z z}$$

Summing up all plane waves with the same fixed θ :

$$\int_0^{2\pi} e^{i(\sin\theta\cdot\cos\varphi\cdot kx + \cos\theta\cdot kx)}\, d\varphi = \int_0^{2\pi} e^{i\cos\varphi k_\perp x} d\varphi \cdot e^{ik_z z} \propto J_0(k_\perp x)\cdot e^{ik_z z}$$

gives axially symmetric Bessel beam propagating along z-axis with invariant transversal intensity profile $|J_0(k_\perp r)|^2$

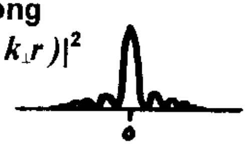

1st experiment: **Durnin, Micely, Eberly,** Phys. Rev. Lett. (1987)

Fig. reproduced from

Y.Lin, W.Seka, J.H.Eberly, H.Huang, D.L.Brown,

Appl.Opt., 31,2708 (1992)

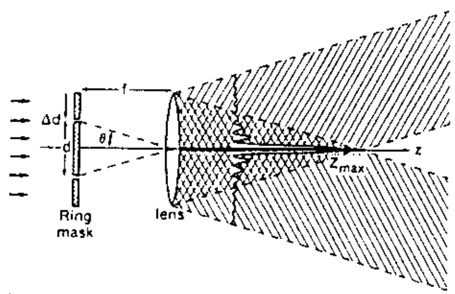

Fig. 1. Schematic setup for generating Bessel beams after Ref. 1.

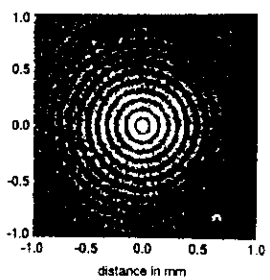

Fig. 2. Typical Bessel beam photograph obtained with a ring aperture of 12.1-mm diameter and 0.1-mm ring width, illuminated by a 1-ns, 1.054-μm, collimated laser pulse from a mode-locker ND:YLF laser. The photograph is taken at 1 m from the 1-m focal length lens (see Fig. 1).

Physically transparent way to get **pulsed versions** of Bessel beams is to integrate over a pulse spectrum S(k):

$$E_{BP}(r,z,t) \;\propto\; \int_0^\infty dk\, S(k)\cdot J_0(k_\perp r)\cdot e^{i(k_z z - \omega t)},$$

$$k = \omega / c \qquad k_\perp = k\sin\theta \qquad k_z = k\cos\theta$$

1. $S_{LX} = \exp\left(\frac{-d_0}{2}\cdot k\right)$
2. $S_G = \exp\left[-\frac{[d_0\cdot(k-k_0)]^2}{2}\right]$
3. $S_{MG} = \frac{k}{k_0}\cdot\exp\left[-\frac{[d_0\cdot(k-k_0)]^2}{2}\right]$

$$\frac{d_0}{c} = 1\cdot 10^{-15}\ \text{sec}$$

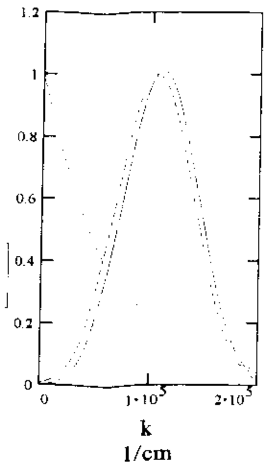

Lu, Greenleaf (1992): "X-wave" (exper. with ultrasound):

$$E_x(r,z,t) \;\propto\; \frac{\frac{1}{2}d_0}{\sqrt{(r\sin\theta)^2 + \left[\frac{1}{2}d_0 - i(z\cos\theta - ct)\right]^2}}$$

For S_{MG} we have found:

$$E_{BX}(r,z,t) \;\propto\; \sqrt{Z(d)}\cdot\exp\left[-\frac{1}{2d_0^2}\left(r^2\sin^2\theta + d^2\right)\right]\cdot J_0[Z(d)\cdot r\,k_0\sin\theta]\cdot$$

$$d \equiv z\cos\theta - ct, \qquad Z(d) \equiv 1 + i\cdot d/d_0^2 k_0 \;.$$

Fig.1. P.Saari, Phys.Rev.Lett.

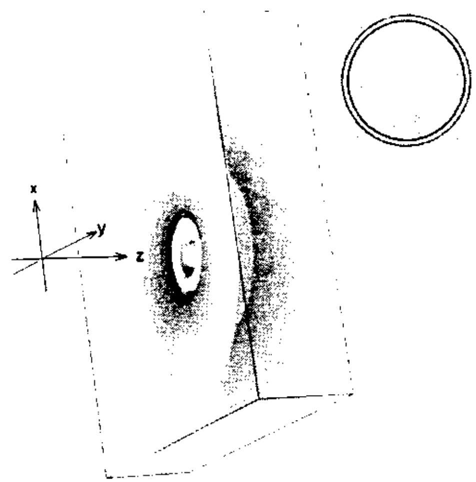

Fig.2. P.Saari, Phys.Rev.Lett.

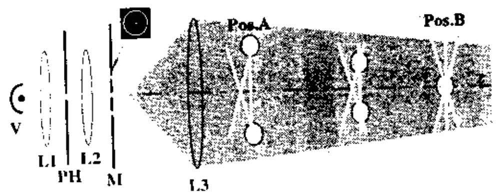

Fig.3. P.Saari, Phys.Rev.Lett.

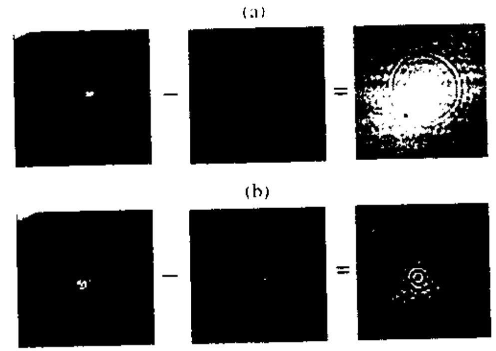

Fig.4. P. Saari, Phys.Rev.Lett.

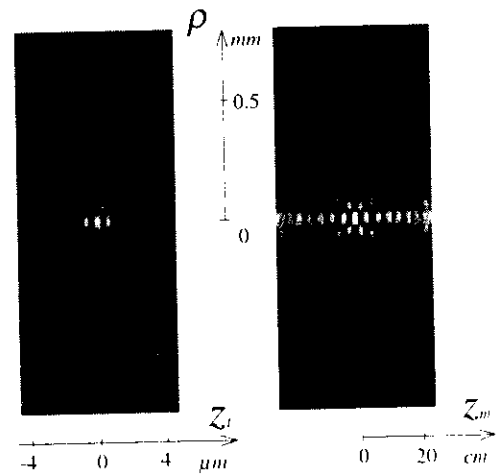

References

Fourier transform and other basic concepts

1. A.V.Oppenheim, A.S. Willsky, and I.T.Young, "Signals and Systems ", *Prentice-Hall,* USA, Englewood Cliffs, 1983.
2. H.Kwakernaak and R.Sivand, "Modern Signals and Systems ", *Prentice-Hall,* USA, Englewood Cliffs, 1990.
3. A.Papoulis, "Pulse compression, fiber communications, and diffraction: a unified approach," (Tutorial), J. Opt. Soc. Am. A 11, 3, 1994.
4. G.A.Korn & T.M.Korn, "Mathematical Handbook for Scientists and Engineers", *McGaw-Hill,* N.Y.-London, 1961

Methods of diagnostics

1. L.Cohen, "Time-frequency distributions – A Review", **Proc. IEEE**, 77, 941, 1989 **(and references therein)**
2. A.Freiberg, P.Saari, "Picosecond spectrochronography", **IEEE J.Quantum Electronics**, QE-19, 622, 1983 **(and references therein).**
3. R.Trebino, K.W.Delong, D.N.Fittinghoff, J.N.Sweetser, M.A.Krumbügel, B.A. Richman, "Measuring ultrashort laser pulses in the time-frequency domain using frequency-resolved optical gating," **Rev. Sci. Instrum**. 68, 3277-3295, 1997 **(and references therein)** (see also `http://www.ca.sandia.gov/ultrafrog`)

Recording, retrieval and design

1. P.Saari, R.Kaarli, A.Rebane, "Picosecond time-and-space-domain holography by photochemical hole burning," **J. Opt. Soc. Amer**. B 3, 527-534, 1986 **(and references therein).**
2. P.Saari, R.Kaarli, M.Rätsep, "Temporally multiplexed Fourier holography and pattern recognition of femtosecond-duration images", **Journal of Luminescence**. 56, 175, 1993 **(and references therein).**
3. H.Sõnajalg, A.Gorokhovskii, R.Kaarli, V.Palm, M.Rätsep, P.Saari, "Optical pulse shaping by filters based on spectral hole burning," **Optics Commun**., 71, 377-380, 1989
4. A.M.Weiner, D.E.Leaird, D.H.Reitze, E.G.Paek, "Femtosecond spectral holography," IEEE **J. Quantum Electronics**, 28, 2251-2261, 1992 **(and references therein).**
5. X.A.Shen, A.-D.Nguyen, J.W.Perry, D.L.Huestis, R.Kachru, "Time-domain holographic digital memory," **Science, 278,** 96-100, 1997 **(and references therein).**
6. P.Saari, K.Reivelt, "Evidence of X-shaped propagation-invariant localized light waves," **Phys. Rev. Lett**., 79, 4135-4138, 1997 **(and references therein).**